Efficient combined SSIM- and landmark-driven image registration in a variational framework

Jorge Larrey-Ruiz[a], Juan Morales-Sánchez[a], Laura Larrey-Ruiz[b]

[a]*Tecnologías de la Información y las Comunicaciones, Universidad Politécnica de Cartagena, 30202 Cartagena, Spain*
[b]*Servicio de Patología Digestiva, Consorcio Hospital General Universitario de Valencia, 46014 Valencia, Spain*

Abstract

Image registration methods are used to establish geometrical correspondences between different datasets. Various characteristics of image data can be exploited to drive image registration algorithms. Thus, the currently available schemes can be roughly divided into two classes: intensity-based and feature-based registration schemes. In this paper, we present a mathematical framework, based on the calculus of variations, for combining these two classes in order to benefit from the advantages of both strategies. The goal is to obtain a registration algorithm which achieves a good matching of datasets near landmark locations but also away from them (by matching the corresponding intensities). The proposed approach includes the novel formulation of a disparity term which simultaneously takes into account the structural similarity index (a similarity measure which considers spatial dependencies in the images) and the location of outstanding points. Since the iteration which results of the variational formulation is translated into the frequency domain, the implementation of the proposed algorithm offers a good speed-performance trade-off when compared to other state-of-the-art image registration implementations. Experimental results show the advantages, in the medical setting, of the combined SSIM- and landmark-based approach over well-established registration techniques which use either landmark or intensity information alone. In particular, the registration of triple-phase 3D computed tomographies of the liver under injection of a contrast agent has been chosen for such a comparison. The datasets are acquired at different times depending on the arrival time of the contrast agent in arteries, portal and hepatic veins, so they have to be registered in order to show the liver structures acquired at each phase in a common framework. These multi-phase studies provide tumor enhancement on the arterial and portal venous phases that support differential diagnosis of lesions in the liver.

Keywords: Image registration, variational methods, Fourier domain, structural similarity index, landmark-driven registration, contrast-enhanced liver CT

1. Introduction

Image registration is the process of finding the spatial correspondence between two different datasets (images or volumes), which typically represent different views of the same object or similar ones; in other words, register is equivalent to *align* in this context. Particularly, in medical imaging there are several applications that require a registration step (e.g. image fusion, atlas matching, pathological diagnosis). Classical reviews of image registration can be found, for example, in the references Brown (1992), Maintz and Viergever (1998), Zitová and Flusser (2003) or Modersitzki (2004). More recent comprehensive overviews about image registration

methods can be found in Sotiras et al. (2015) and Sotiras et al. (2013), where the state-of-the-art advances in this field are described in a systematic fashion, and the techniques applied to medical datasets are emphasized as well. When classified according to the image characteristics used to estimate the transformation which geometrically relates the involved datasets, registration algorithms are usually divided into three groups: geometric feature-based, which rely on the segmentation, done generally before the registration process itself, of part or all of the images, therefore obtaining objects that are registered by minimizing some geometrical distance between them; intensity-based, which maximize a intensity similarity measure computed between points lying at the same spatial position; and iconic feature-based, which can be understood as intermediate between the two previous categories, since they use explicitly some type of geometrical distance in addition to the intensity similarity measure, see Cachier et al. (2003). The performance of intensity-based image registration methods is highly influenced by the choice of the similarity measure. This measure can be defined directly on image intensities as, e.g., sum of squared differences (SSD), correlation coefficient (CC), correlation ratio (CR), or mutual information (MI). A complete analysis of all these metrics can be found in Loizou et al. (2014). These measures often rely on the assumption of independence and stationarity of the intensities from pixel to pixel without considering their spatial dependencies. Alternative metrics have been proposed in order to consider intensity nonstationarities and complex spatially-varying intensity distortions. For instance, in Myronenko and Song (2010) a similarity measure based on the residual complexity is described. Another example is the structural similarity index (SSIM), introduced by Wang et al. (2004), which achieves a good trade-off between speed and performance and is able to cope with complex relationships between image intensity values. Due to the mathematical properties of SSIM (Brunet et al., 2012) and its potentials in both theoretical development and practical applications, it is being incorporated into optimization frameworks in order to improve perceived image/video quality in a number of image processing problems, as e.g. Huang et al. (2010) or Rehman et al. (2011). This similarity measure has been previously used in image registration in Ben Sassi et al. (2008), Amintoosi et al. (2009), Vishnukumar and Wilscy (2009), Wang and Zhang (2009), Wirth and Bobier (2009), or Kalinic et al. (2011), but its use is still not widespread —for example, the evaluation addressed in Ou et al. (2014) does not include SSIM and the review in Sotiras et al. (2013) does not deal with similarity measures based on the SSIM—.

Intensity-based approaches are in general fully automatic and usually yield good registration results. However, they may perform poorly for specific, important locations such as anatomical landmarks. On the other hand, geometric feature-based registration techniques are designed to accurately match user specified landmarks, see e.g. Rohr (2001). Recent examples of landmark-based registration methods in medical imaging scenarios can be found in Wen et al. (2015) or Kolesov et al. (2016). A common drawback of most landmark-driven registration methods is the fact that the intensities of the datasets are completely neglected. Consequently, the registration outcome away from the landmarks may be very poor. In the literature, the registration results are typically obtained by interpolating the transformation with a *thin-plate spline* (TPS) model (Bookstein, 1989) or by combining iterative closest point (ICP) registration and parametric relaxation (Tosun et al., 2004), among other techniques. Although these approaches produce a smooth transformation from one dataset to another, they do not define a consistent correspondence between the two datasets except at the landmark points. Some previous attempts to combine the sparse correspondences with a intensity-based registration method can be found in Johnson and Christensen (2002) or Urschler et al. (2006). However, to the authors knowledge, there has been no attempt to formulate a registration method which combines in the distance term both a SSIM-

based term and a landmark-based term. In recent works, such as Naranjo et al. (2015) or Legaz-Aparicio et al. (2017), the authors of this paper dealt with intensity-based registration approaches within the variational framework first presented in Larrey-Ruiz et al. (2008), whose formulation in the frequency domain allowed for implementations of high efficiency (Verdú-Monedero et al., 2008). Please refer to Amit (1994) or Zhang et al. (2006) for further details regarding variational image registration. The aforementioned approaches involved similarity terms derived from SSD- or CR-based measures, so none of them included a SSIM-based nor a landmark-based distance term. Regardless, the method presented in Legaz-Aparicio et al. (2017) achieved better results than publicly available state-of-the art approaches such as *Elastix* (Klein et al., 2010) and ANTs (`http://stnava.github.io/ANTs/`).

The paper is organized as follows: Section 2 addresses the formulation, within the variational framework, of a novel registration method which combines in the distance term both a SSIM-based term and a landmark-based term. Section 3 shows the results of applying the proposed registration algorithm to a medical imaging scenario; in particular, the image registration of triple-phase 3D computed tomography datasets of the liver under injection of a contrast agent has been chosen; the suitability of our approach in such a scenario is also proved in this section through the comparison of the results it provides and the outcome obtained with the CR-based version of the algorithm, which was recently reported to outperform other well-known approaches in the medical setting (Legaz-Aparicio et al., 2017). The conclusions of the paper as well as the future lines of research are discussed in Section 4. Finally, an appendix closes the paper with the detailed derivation of the external forces field related to the proposed SSIM-based distance term (i.e., the first addend of the corresponding Euler-Lagrange equation).

2. Mathematical framework

Let R and T be two datasets, a reference and a template respectively, which represent the same object (or similar ones) by using the same or different imaging modalities. These d-dimensional datasets are defined as $R, T : \Psi \to \mathcal{I}$, with $\Psi \subset \mathbb{R}^d$ being the domain where they are supported, and $\mathcal{I} \subset \mathbb{R}$ representing the intensity level in each spatial coordinate $\mathbf{x} = (x_1, \dots, x_d)$. We search for a displacement field $\mathbf{u} : \Psi \to \mathbb{R}^d$ that makes the transformed template $T_{\mathbf{u}} : \Psi \to \mathcal{I}$ similar to the reference dataset in the geometrical sense, i.e., $\mathbf{x}_{T_{\mathbf{u}}} = \mathbf{x}_T + \mathbf{u}(\mathbf{x}_T) \approx \mathbf{x}_R$, where $\mathbf{u}(\mathbf{x}) = (u_1(\mathbf{x}), \dots, u_d(\mathbf{x}))^\top$. This problem can be approached in terms of the variational calculus by defining a joint energy functional to be minimized:

$$\mathcal{J}[\mathbf{u}] = \mathcal{D}[R, T; \mathbf{u}] + \alpha \, \mathcal{S}[\mathbf{u}], \tag{1}$$

where $\mathcal{D}$ is an energy term which quantifies the disparity between the datasets, $\mathcal{S}$ is a penalty term which measures the roughness of the solution $\mathbf{u}(\mathbf{x})$, and $\alpha > 0$ is a scalar parameter, usually referred to as the regularization parameter, which is used to control and weight the influence of the penalty term versus the distance term. It should be noted that the present formulation considers the different functions to be continuous in the domain Ψ where they are supported; the natural spatial (and temporal) discretization is tackled later in this section.

In the literature, several choices for the dissimilarity measure $\mathcal{D}$ can be found. Depending on the particular datasets to be compared, statistical measures derived from the MI or the CR are usually the most appropriate candidates. As an alternative, in this work we propose the novel approach of incorporating both the SSIM (Wang et al., 2004) and the Euclidean distance between

identifiable corresponding points (i.e., landmarks) into the variational framework which is being presented. The resulting disparity term is the following:

$$\mathcal{D}[R, T; \mathbf{u}] = \frac{-(2\,\mu_R\,\mu_T + C_1)(2\,\sigma_{RT} + C_2)}{(\mu_R^2 + \mu_T^2 + C_1)(\sigma_{RR} + \sigma_{TT} + C_2)} + \frac{\beta}{2} \int_{\mathbf{\Psi}} \sum_{j=1}^{N} \left\| \mathbf{x}_{R_j} - \mathbf{x}_{T_j} - \mathbf{u}(\mathbf{x}_{T_j}) \right\|^2 d\mathbf{x}, \quad (2)$$

where μ_R, μ_T, σ_{RR} and σ_{TT} denote the mathematical expectations and variances of the intensity levels of R and $T_{\mathbf{u}}$, respectively; σ_{RT} represents the covariance; C_1 and C_2 are small constants which aim to characterize the saturation effects of the visual system at low luminance and contrast regions and which assure numerical stability when the expectations or variances are very close to zero; $\beta > 0$ is a scalar used to weight the influence of the landmark-based term versus the SSIM-based term; N is the number of identified landmarks; and $\mathbf{x}_{R_j}$ and $\mathbf{x}_{T_j}$ denote the spatial position of the j-th landmark in R and T, respectively.

The regularization term $\mathcal{S}$ is used to add some prior knowledge on the displacement field, thus preferentially obtaining more likely solutions and giving the smoothness characteristics to $\mathbf{u}(\mathbf{x})$. In this work, the regularizer is defined by

$$\mathcal{S}[\mathbf{u}] = \frac{1}{2} \sum_{l=1}^{d} \int_{\mathbf{\Psi}} \left\| \nabla^{\lambda} u_l \right\|^2 d\mathbf{x}, \quad (3)$$

where ∇ denotes the d-dimensional gradient operator, and $\lambda \in \{1, 2\}$ is the regularization order: if $\lambda = 1$, the resulting term is the diffusion smoother (Fischer and Modersitzki, 2002); if $\lambda = 2$, the regularizer is the curvature smoother (Fischer and Modersitzki, 2004).

According to the variational calculus, a necessary condition for a minimizer $\mathbf{u}$ of the joint energy functional (1) is that the first variation of $\mathcal{J}[\mathbf{u}]$ in any direction (also known as the *Gâteaux* derivative) vanishes for all possible perturbations $\mathbf{z} \in \mathbb{R}^d$:

$$\mathrm{d}\mathcal{J}[\mathbf{u}; \mathbf{z}] = \frac{\partial}{\partial \epsilon} \mathcal{J}[\mathbf{u} + \epsilon \mathbf{z}] \Big|_{\epsilon=0} = 0, \quad \forall \mathbf{z} \in \mathbb{R}^d. \quad (4)$$

The computation of the previous *Gâteaux* derivative leads to the following Euler-Lagrange (E-L) equation:

$$\frac{1}{\mathcal{V}_{\mathbf{\Psi}}} \left(\hat{G}_{\rho} * \frac{\partial L_{\mathbf{u}}^{\mathrm{SSIM}}}{\partial i_t} \right) \nabla T_{\mathbf{u}} + \beta \sum_{j=1}^{N} \left(\mathbf{x}_{T_{\mathbf{u}j}} - \mathbf{x}_{R_j} \right) + \alpha \, (-\Delta)^{\lambda} \mathbf{u} = \mathbf{0}, \quad (5)$$

where $\mathcal{V}_{\mathbf{\Psi}}$ represents the hypervolume of $\mathbf{\Psi}$; $\hat{G}_{\rho} : \mathcal{I}^2 \to \mathbb{R}$ is a Gaussian kernel (strictly positive and differentiable); $*$ denotes the d-dimensional convolution operator; Δ is the Laplacian operator; finally, we find the term

$$\frac{\partial L_{\mathbf{u}}^{\mathrm{SSIM}}}{\partial i_t} = \frac{\gamma_0 + C_1\,\gamma_1 + C_2\,\gamma_2 + C_1 C_2\,\gamma_3}{(\mu_R^2 + \mu_T^2 + C_1)^2 (\sigma_{RR} + \sigma_{TT} + C_2)^2}, \quad (6)$$

where the variables γ_0, γ_1, γ_2 and γ_3 are defined as

$$\gamma_0 = 4\mu_R \big(\mu_R^2(\sigma_{RR}\,\sigma_{RT} + \sigma_{TT}\,\sigma_{RT} - \mu_R\,\mu_T\,\sigma_{RR} - \mu_R\,\mu_T\,\sigma_{TT} + 2\mu_T^2\,\sigma_{RT} + \mu_T\,\sigma_{RR}\,i_r + \mu_T\,\sigma_{TT}\,i_r - 2\mu_T\,\sigma_{RT}\,i_t)$$

$$- \mu_T^2(\sigma_{RR}\,\sigma_{RT} + \sigma_{TT}\,\sigma_{RT} + \mu_R\,\mu_T\,\sigma_{RR} + \mu_R\,\mu_T\,\sigma_{TT} - 2\mu_T^2\,\sigma_{RT} - \mu_T\,\sigma_{RR}\,i_r - \mu_T\,\sigma_{TT}\,i_r + 2\mu_T\,\sigma_{RT}\,i_t) \big),$$

$$(7)$$

4

$$\gamma_1 = 2\big(\mu_R(-\mu_R^2\,\sigma_{RR} - \mu_R^2\,\sigma_{TT} + 2\,\sigma_{RR}\,\sigma_{RT} + 2\,\sigma_{TT}\,\sigma_{RT} + \mu_R\,\sigma_{RR}\,i_r + \mu_R\,\sigma_{TT}\,i_r - \sigma_{RR}\,C_1 - \sigma_{TT}\,C_1)$$
$$- \mu_T(2\,\mu_R^2\,\sigma_{RR} + 2\,\mu_R^2\,\sigma_{TT} + \mu_R\,\mu_T\,\sigma_{RR} + \mu_R\,\mu_T\,\sigma_{TT} - 2\,\mu_R\,\sigma_{RR}\,i_r - 2\,\mu_R\,\sigma_{TT}\,i_r - \mu_T\,\sigma_{RR}\,i_r - \mu_T\,\sigma_{TT}\,i_r)$$
$$+ 2\,\mu_T\,\sigma_{RT}(\mu_R^2 + \mu_T^2 - \sigma_{RR} - \sigma_{TT} + 2\,\mu_R\,\mu_T - 2\,\mu_R\,i_t - \mu_T\,i_t + C_1) + C_1\,i_r(\sigma_{RR} + \sigma_{TT}) - 2\,\sigma_{RT}\,i_t(\mu_R^2 + C_1)\big),$$

$$\tag{8}$$

$$\gamma_2 = 2\,\mu_R\big(\mu_R^2(\sigma_{RR} + \sigma_{TT} + 2\,\sigma_{RT} - 2\,\mu_R\,\mu_T + 2\,\mu_T^2 + 2\,\mu_T\,i_r - 2\,\mu_T\,i_t + C_2)$$
$$- \mu_T^2(\sigma_{RR} + \sigma_{TT} + 2\,\sigma_{RT} + 2\,\mu_R\,\mu_T - 2\,\mu_T^2 - 2\,\mu_T\,i_r + 2\,\mu_T\,i_t + C_2)\big),$$

$$\tag{9}$$

$$\gamma_3 = 2\big(\mu_R(\sigma_{RR} + \sigma_{TT} - 2\,\sigma_{RT} - \mu_R^2 + \mu_T^2 + \mu_R\,i_r - \mu_R\,i_t + 2\,\mu_T\,i_r + C_2)$$
$$- \mu_T(\sigma_{RR} + \sigma_{TT} + 2\,\sigma_{RT} + \mu_R^2 - \mu_T^2 + 2\,\mu_R\,i_t - \mu_T\,i_r + \mu_T\,i_t - C_1 + C_2) - C_1\,i_t\big),$$

$$\tag{10}$$

with $i_r, i_t \in \mathcal{I} \subset \mathbb{R}$ being the intensities of R and $T_{\mathbf{u}}$, respectively.

In Appendix A, the first addend in equation (5) is deduced. The proof of the internal forces field of the Euler-Lagrange equation (i.e., the last addend in eq.(5)) can be found in Larrey-Ruiz et al. (2007). Finally, the addend which corresponds to the landmark-based term can be easily obtained by applying the definition of the *Gâteaux* derivative to the last addend in eq.(2):

$$d\mathcal{D}^{\mathrm{LM}}[R, T; \mathbf{u}; \mathbf{z}] = \frac{\partial}{\partial\epsilon}\frac{\beta}{2}\int_{\boldsymbol{\Psi}}\sum_{j=1}^{N}\left\|\mathbf{x}_{R_j} - \mathbf{x}_{T_j} - \mathbf{u}(\mathbf{x}_{T_j}) - \epsilon\mathbf{z}(\mathbf{x}_{T_j})\right\|^2 d\mathbf{x}\Big|_{\epsilon=0}$$

$$= \int_{\boldsymbol{\Psi}}\Big\langle\beta\sum_{j=1}^{N}\mathbf{x}_{R_j} - \mathbf{x}_{T_j} - \mathbf{u}(\mathbf{x}_{T_j}) - \epsilon\mathbf{z}(\mathbf{x}_{T_j}), -\mathbf{z}(\mathbf{x}_{T_j})\Big\rangle_{\mathbb{R}^d}d\mathbf{x}\Big|_{\epsilon=0} = \int_{\boldsymbol{\Psi}}\Big\langle\beta\sum_{j=1}^{N}\big(\mathbf{x}_{T_{\mathbf{u}j}} - \mathbf{x}_{R_j}\big), \mathbf{z}(\mathbf{x}_{T_j})\Big\rangle_{\mathbb{R}^d}d\mathbf{x},$$

$$\tag{11}$$

where $\langle\cdot,\cdot\rangle_{\mathbb{R}^d}$ denotes the inner (or *dot*) product in $\mathbb{R}^d$.

In order to solve the Euler-Lagrange equation (5), an iterative time-marching scheme can be used. For doing so, an artificial time t has to be added to the E-L equation and then the steady-state solution has to be computed, i.e., $\frac{\partial}{\partial t}\mathbf{u} + \mathbf{f} + \alpha(-\Delta)^\lambda\mathbf{u} = \mathbf{0}$ (where $\mathbf{f}$ gathers the first two addends in eq.(5)). In the steady-state, the displacement field $\mathbf{u}$ converges and hence $\frac{\partial}{\partial t}\mathbf{u} = \mathbf{0}$. The time t is discretized, $t = \xi\tau$ (with $\xi \in \mathbb{N}$ being the iteration index and where $\tau > 0$ is the time-step), and finally the temporal derivative is replaced with its discrete approximation (first backward difference). Due to the fact that digital datasets are usually encoded by uniformly distributed spatial elements in each dimension (e.g. pixels if $d = 2$ or voxels if $d = 3$), the discretization of the spatial variable becomes a natural approach too. Therefore in the following the notation $\mathbf{u}^{(\xi)}[\mathbf{n}] = \mathbf{u}[\mathbf{n}, \xi\tau]$ is used, where $\mathbf{n} = (n_1, \ldots, n_d)$ is the index of the discrete spatial position, with $n_i = 0, \ldots N_i - 1$, and N_i being the number of discrete spatial elements in the i-th dimension. Using this notation, the resulting semi-implicit iteration for the l-th component of the displacement field is the following:

$$u_l^{(\xi)}[\mathbf{n}] = u_l^{(\xi-1)}[\mathbf{n}] - \tau f_l^{(\xi-1)}[\mathbf{n}] - \tau\alpha\, q[\mathbf{n}] * u_l^{(\xi)}[\mathbf{n}], \tag{12}$$

where the discrete operator $q[\mathbf{n}]$ stands for a kernel which performs the discrete approximation of the spatial derivatives of $(-\Delta)^\lambda$.

As an alternative to the spatial approach, solving the iteration (12) in the frequency domain provides a stable implementation for the computation of a numerical solution for the displacement field $\mathbf{u}[\mathbf{n}]$, and in a more efficient way than other existing approaches if the d-dimensional

fast Fourier transform (FFT) is taken into account (Verdú-Monedero et al., 2008). Translating the semi-implicit iteration (12) into the frequency domain results in

$$U_l^{(\xi)}(\omega) = U_l^{(\xi-1)}(\omega) - \tau F_l^{(\xi-1)}(\omega) - \tau \alpha Q(\omega) U_l^{(\xi)}(\omega), \tag{13}$$

where $U_l^{(\xi)}$, $U_l^{(\xi-1)}$ and $F_l^{(\xi-1)}$ are the d-dimensional Fourier transforms of $u_l^{(\xi)}$, $u_l^{(\xi-1)}$ and $f_l^{(\xi-1)}$, respectively, and $\omega = (\omega_1, \ldots, \omega_d)$ is the d-dimensional counterpart in the frequency domain associated to the discrete spatial variable $\mathbf{n}$. The operator $Q(\omega)$ performs the spatial derivatives in the frequency domain and allows for their calculation by means of the product of spectra (i.e., the translation of the spatial convolution into the frequency domain); as deduced in Verdú-Monedero et al. (2008), its analytical expression is the following:

$$Q(\omega) = \left(2 \sum_{m=1}^{d} (1 - \cos \omega_m)\right)^\lambda. \tag{14}$$

It should be noted that, mathematically, any value $\lambda \in [1, 2]$ makes sense in the frequency domain (but not in the spatial domain). This allows for the design of *hybrid* diffusion-curvature regularizers with adaptable properties, please refer to Larrey-Ruiz et al. (2008) for further details.

As explained in previous paragraphs, it is taken into account that the datasets are discrete and then the spatial variable $\mathbf{x}$ gives rise to the discrete spatial index $\mathbf{n}$. Similarly, instead of handling continuous spectra, the frequency domain is also discretized and only the N_m uniformly sampled frequencies $\omega_m = (0, \frac{2\pi}{N_m}, \ldots, \frac{2\pi}{N_m}(N_m - 1))$ are evaluated in each dimension. This way the iteration (13) can be implemented efficiently using the fast algorithms for the computation of the DFT which are provided by many programming languages (e.g., MATLAB's `fftn` built-in function which is based on the FFTW library by Frigo and Johnson (2005)).

Finally, the iteration of the proposed registration algorithm is the following:

$$u_l^{(\xi)}[\mathbf{n}] = \text{IFFT}\left\{H[\mathbf{k}] \, \text{FFT}\{u_l^{(\xi-1)}[\mathbf{n}] - \tau f_l^{(\xi-1)}[\mathbf{n}]\}\right\}, \tag{15}$$

where $H[\mathbf{k}] = (1 + \tau \alpha Q[\mathbf{k}])^{-1}$, $Q[\mathbf{k}] = (2 \sum_{m=1}^{d} (1 - \cos(\frac{2\pi}{N_m} k_m)))^\lambda$, $\mathbf{k} = (k_1, \ldots, k_d)$, and $k_m = 0, \ldots, N_m - 1$. Due to the fact that $Q[\mathbf{k}]$ results in a circulant block matrix, all the spectra products and pseudo-inversions become Hadamard (i.e., pointwise) products and divisions, respectively (Davis, 1979).

3. Results

In order to assess the performance of the proposed methodology, it is tested on 15 medical experiments involving triple-phase 3D computed tomography (CT) volumes of the liver under contrast agent injection. Although the acquisition of the different phases is continuous in most cases, there is no exact correspondence between them, so they must be registered in order to show the results in a common 3D framework. First, a study without contrast agent is acquired. Once the contrast agent is injected, it reaches the arteries (arterial phase), then the portal veins and next the hepatic veins. Hepatic and portal veins are then visible in the portal venous phase. Image registration allows to locate exactly the vessels in 3D at each phase of contrast-enhanced CT data in order to measure distances and volumes and provide objective parameters of the pathology which facilitate comparisons between patients, the tracking of tumors (Charnoz et al., 2005), to make calculations on the volume of the liver to be preserved prior to a liver resection
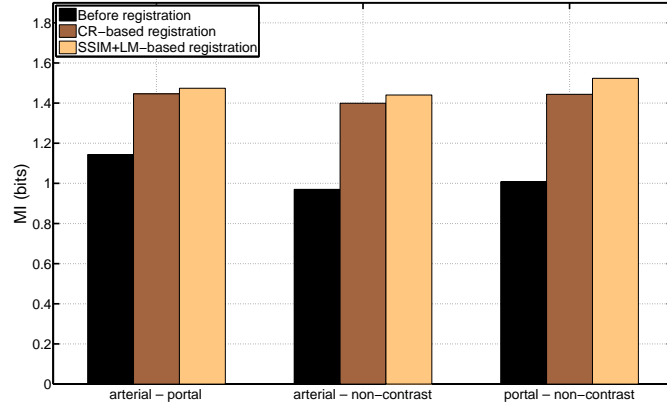
Figure 1: Mean similarity between images in terms of mutual information for the three considered scenarios (arterial-portal, arterial-non-contrast and portal-non-contrast) before and after the registration.

(a) Box plot of the registration error
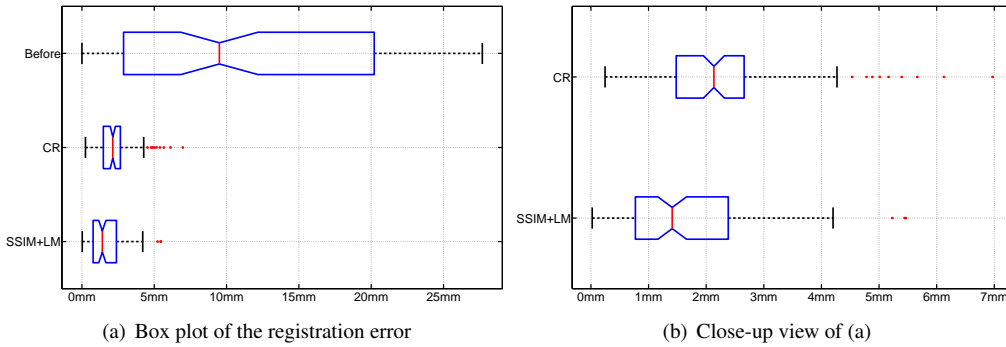
(b) Close-up view of (a)

Figure 2: Spatial distances (in millimeters) between corresponding landmarks before and after the registration process.

(Elhawary et al., 2009), or to generate vessel models for planning surgical procedures (Lange et al., 2005). The experiments carried out involve data from 5 patients. The acquisition device is a GE LightSpeed VTC (General Electric Medical Systems). The size of the volumes vary from $512 \times 512 \times 34$ to $512 \times 512 \times 51$ voxels, with a resolution of $0.9102 \times 0.9102 \times 5$ millimeters.

For the assessment of the proposed method, we carry out a comparison with the purely intensity-based variational method recently presented by the authors of this work in Legaz-Aparicio et al. (2017). This CR-based approach was reported to outperform publicly available state-of-the art methods such as *Elastix* and ANTs in the medical setting. As can be seen in Fig.1, the proposed framework shows excellent results for the three considered registration scenarios (arterial-portal, arterial-non-contrast and portal-non-contrast), reaching average values of 1.47, 1.44 and 1.52 bits in terms of mutual information, corresponding to the arterial-portal, arterial-non-contrast and portal-non-contrast cases, respectively; this represents a mean improvement of 28.9%, 48.45% and 51.16% in relative terms of mutual information, thus outperforming the CR-based registration algorithm, which achieves a mean improvement of 26.48%, 44.22% and

7

(a) Arterial phase (reference dataset, R)

(b) Non-contrast phase (template dataset, T)

(c) Registered template, $T_{\mathbf{u}}$ (CR-based method)

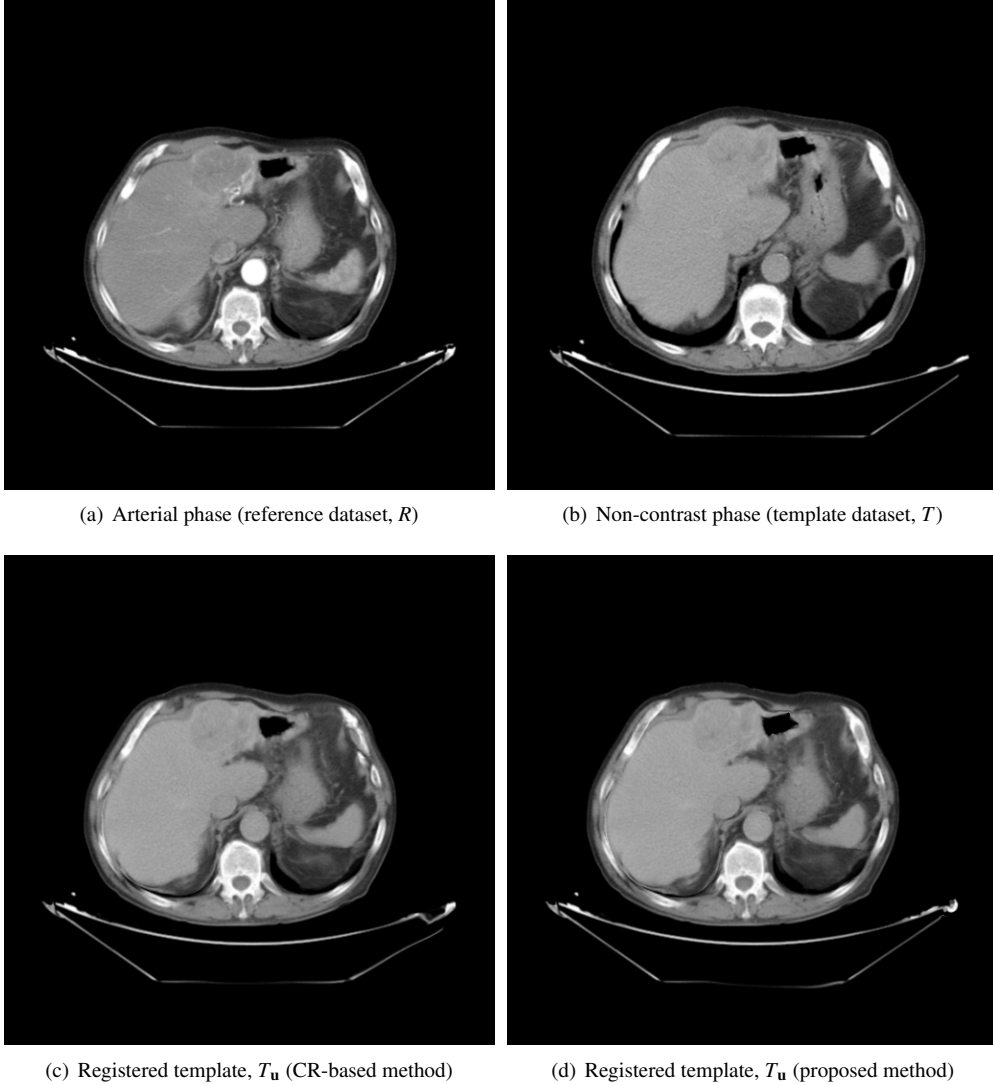(d) Registered template, $T_{\mathbf{u}}$ (proposed method)

Figure 3: Visual outcomes of experiment #1 (slice #9): registration of arterial and non-contrast phases of patient #1.

43.25%, respectively. Additionally, due to the analogous behavior (i.e., comparable final values of mutual information) of the proposed method in the three scenarios, all available experiments can be grouped into one ensemble in order to assess a more comprehensive validation of the actual registration error. A ground truth was established by an expert in the form of identifiable anatomical locations (landmarks) for all experiments. The registration errors were then obtained by computing the spatial distance between the corresponding landmarks in the reference and registered template datasets. Figures Fig.2(a) and Fig.2(b) show through box plots the registration error (in millimeters) achieved by the methods under comparison, gathering the results from

(a) Arterial phase (reference dataset, R)

(b) Portal venous phase (template dataset, T)

(c) Registered template, $T_{\mathbf{u}}$ (CR-based method)

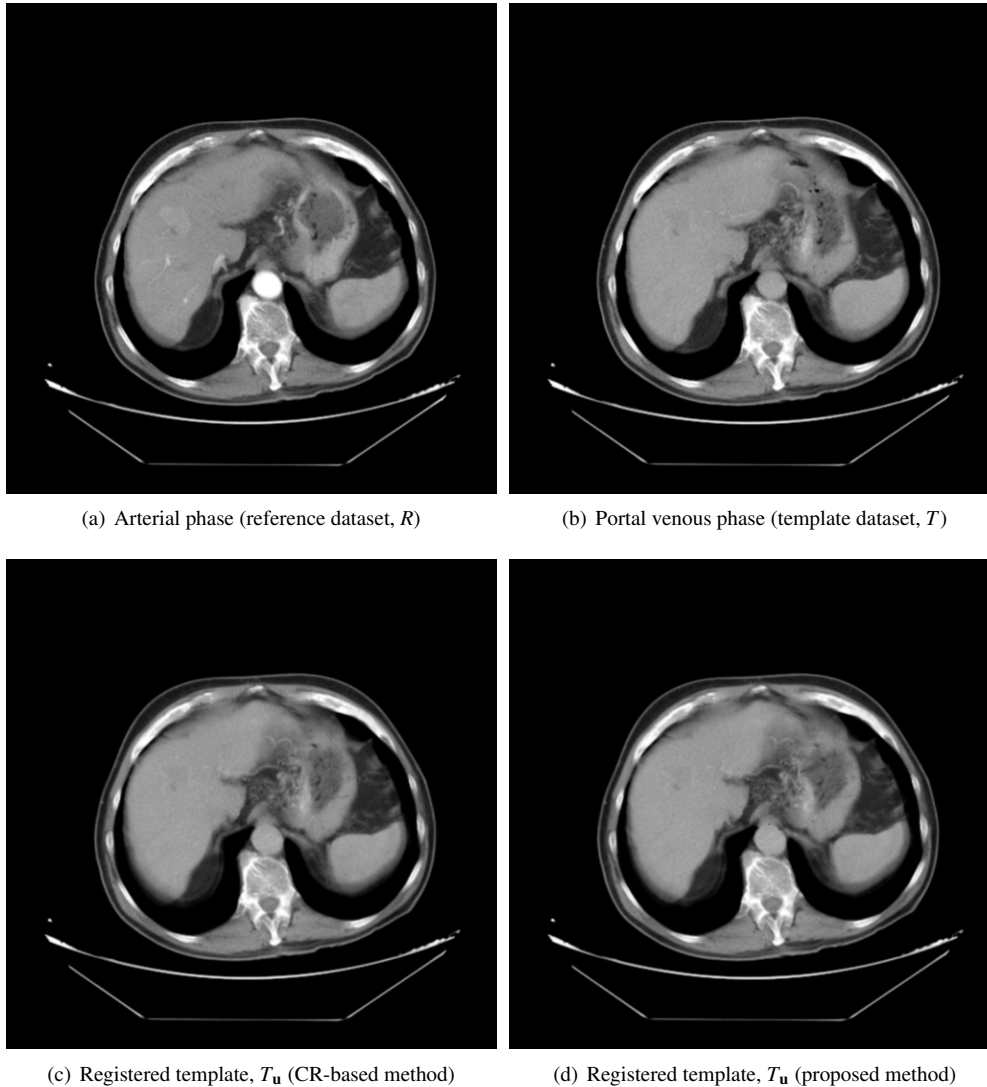(d) Registered template, $T_{\mathbf{u}}$ (proposed method)

Figure 4: Visual outcomes of experiment #5 (slice #12): registration of arterial and portal venous phases of patient #2.

the three considered registration scenarios. These box plots collect the final spatial distances between corresponding landmarks, along with the median distance error and its statistical significance (notch showing the 95% confidence interval of the true median). According to Fig.2(b), the proposed method significantly improves on the registration error of the CR-based approach, since it reduces the initial median error from 9.50 mm to a residual median distance between landmarks of 1.41 mm, decreasing at the same time the outliers occurrence.

In addition to the previous measurements, the visual outcomes of two of the experiments are shown in figures Fig.3 and Fig.4, whose purpose is to highlight the most illustrative differences

Size	CR	SSIM+LM	*Elastix*
$512 \times 512 \times 16$	2.40	2.52	5.69
$512 \times 512 \times 32$	5.03	5.27	11.20
$512 \times 512 \times 64$	10.42	10.93	22.01

Table 1: Mean execution time per iteration (in seconds) of the considered variational methods and *Elastix*, involving datasets of different sizes. These times were obtained on a PC with Intel Core i5-2500K, 3.3 GHz, 16 GB RAM, running Windows 8.1 (64 bits). All methods have been implemented in C++.

(from a medical point of view) between the results provided by the compared methods. In Fig.3, we observe a normal size of the liver, with discretely irregular contours and homogeneous signal intensity. In hepatic segment II, there is a lesion of 40 mm of maximum axis, encapsulated and with well-defined contours and heterogeneous enhancement in arterial phase (after administration of intravenous contrast), suggestive of hepatocellular carcinoma (HCC). In this slice of the CT scan, we can also observe the aorta that shines in the arterial phase, the lower area of the stomach and the upper area of the spleen. In Fig.4, the liver has a normal size with discretely irregular contours in relation to changes due to chronic liver disease. In hepatic segment IV, a 36 mm diameter focal lesion is identified, which has arterial phase enhancement with a small area of necrosis of 13 mm; it corresponds to a HCC previously chemoembolized with partial necrosis. In this slice of CT, we can also observe the aorta, the gastric chamber and the spleen. When comparing the two methods under study, it can be seen how in Fig.3 the resulting registered datasets are very similar. However, looking closely, it can be noticed that in the right part of the image (left side of the patient) the shape and width of the structures corresponding to the stomach and the spleen in Fig.3(d) match better those in the reference dataset. Likewise, the part of the rib at the upper right of the image is more similar to the same region in the reference dataset by using the proposed method. Regarding the experiment shown in Fig.4, it can be easily appreciated how the geometrical matching (with respect to the reference dataset, Fig.4(a)) of the structures in the right side of the image (specially the gastric chamber) is visually more satisfactory in Fig.4(d). Moreover, the area of tumor necrosis which results from the proposed method is also slightly better aligned.

Throughout this work, the SSIM-based term uses the following parameters setting: $C_1 = 0.01$ and $C_2 = 0.03$. These are the empirically obtained values suggested in the reference paper Wang et al. (2004). Regardless, we find that in the current scenario, the performance of the proposed registration algorithm is fairly insensitive to variations of these values. Regarding the remaining parameters, which are exclusively related to our variational approach, the values of $\lambda = 2$ (i.e., curvature smoother, since the deformations to be corrected are notable in some cases), $\alpha = 200$, $\beta = 5$ (only applicable to the combined SSIM- and landmark-based method) and $\tau = 1$ were used for all experiments —we recommend a common set which achieves a good balance between generalization and performance—. This parameter setting was obtained following the guidelines first introduced in Larrey-Ruiz and Morales-Sánchez (2006). As for the number of iterations, a value of $\xi_{max} = 80$ grants convergence in all cases; the cost function stabilizes after $50-70$ iterations for both the CR-based and the proposed algorithm. From the results gathered in Table 1, it can be concluded that the computational overhead introduced by the novel approach does not increase significantly the execution time of the CR-based algorithm. Moreover, both variational approaches outperform well-established registration methods such as *Elastix* in terms of efficiency. *Elastix* was the fastest method which provided better results among

the open source methods of image registration which entered in the second phase of Empire10 Challenge (Murphy et al., 2011). The overall complexity of each iteration of the compared algorithms is $O(N)$ —where N is the number of voxels of the datasets—, since doubling N means doubling the computational time.

4. Conclusions and discussion

In this work, a theoretical framework has been presented for approaching the image registration problem. In particular, we have formalized the variational formulation of image registration, making it valid even for a general d-dimensional case. The resulting semi-implicit iteration, which is solved in the frequency domain, allows for an efficient implementation if fast algorithms for the computation of the DFT are taken into account. The main novelty of this paper lies in the inclusion within such a framework of a disparity energy which combines the information provided by both the structural similarity index (SSIM) and the location of geometrical identifiable points (landmarks). With this purpose, the corresponding external forces fields of the resulting Euler-Lagrange equation have been deduced, and their analytical expressions are explicitly provided.

The suitability of the proposed methodology in the medical setting has been validated by means of illustrative experiments involving liver CT data under different contrast agent injection. When compared with an intensity-based method which was recently reported to outperform other popular state-of-the-art methods, it has been shown that the novel approach achieves higher values for both the similarity measure considered (mutual information) and the actual registration error (distance in space between corresponding landmarks). Moreover, the results provided by the method proposed in this paper are subjectively considered more satisfying after being visually inspected by an expert. However, the main advantage of the proposed registration method is its efficiency. As expected, the FFT-based, C++ implementation of our approach outperforms fast methods such as *Elastix* in terms of computational cost, while keeping the execution times in the range of its main contestant (the previously proposed CR-based algorithm). In a clinical environment, where computational times should be kept as low as possible, this feature can be of paramount importance. Regardless, it should be noted that comparing the performance of different image registration algorithms is not a trivial task, since each approach has its own set of user-defined parameters, which may heavily influence the final outcome. For instance, if they are tested on datasets with different characteristics (e.g., modality or anatomical region), new optimal parameters need to be determined. In this sense, open challenges are an interesting way to categorize image registration software packages in a common context.

It should be noted that the proposed method considers the input directional field as a periodic signal. Unless this is taken into account, the vectors located near the boundaries will be erroneous. As stated by other authors —see e.g. Fischer and Modersitzki (1999)—, this is hardly a problem if the data is contained within a uniform background (e.g., when dealing with medical images or volumes, as in the current scenario), or else it can be overcome by using a folded algorithm which extends the dataset symmetrically, thus resulting in additional reflections of the original input, see e.g. Bai and Feng (2007).

The most notable limitation of the present method is that the SSIM-based term would not be an appropriate choice for the combined disparity energy unless matching voxels of the datasets have similar intensities (i.e., in pure monomodal or pseudo-monomodal scenarios). In fact, this is an inherent drawback of the structural similarity index, not a problem which arises with our methodology. However, even if the aim was to register multimodal datasets, one could still use

11

the proposed variational approach, but considering an alternative distance term instead (e.g., a combined CR- and landmark-based disparity energy).

In ongoing research, we would like to address the application of our methodology to other scenarios, such as the fusion of datasets from different modalities: for example, anatomical (CT and MRI), metabolic (spectroscopic MRI and PET) and functional (f-MRI) volumes in the medical setting. Alternative definitions of the joint functional, including additional energy terms —e.g., a measure of the differences between forward and reverse transformations, so that the resulting displacement field is *consistent*—, are currently being explored within the presented theoretical framework.

Appendix A. Variational formulation of SSIM

In this work, we propose the opposite of the structural similarity index as the intensity-based part of the disparity term of the joint energy functional (first addend in equation (2)). Thus, a maximization problem is transformed into the minimization of the following cost function:

$$\mathcal{D}^{\text{SSIM}}[R, T; \mathbf{u}] := -\text{SSIM}[R, T_{\mathbf{u}}] = \frac{-(2\,\mu_R\,\mu_T + C_1)(2\,\sigma_{RT} + C_2)}{(\mu_R^2 + \mu_T^2 + C_1)(\sigma_{RR} + \sigma_{TT} + C_2)}\,. \tag{A.1}$$

The mathematical expectations, variances and covariance μ_R, μ_T, σ_{RR}, σ_{TT} and σ_{RT} are defined as follows:

$$\mu_R = \text{E}\{R\} = \int_{\mathcal{I}} i_r\, p_R(i_r) di_r\,, \tag{A.2}$$

$$\mu_T = \text{E}\{T_{\mathbf{u}}\} = \int_{\mathcal{I}} i_t\, p_{T_{\mathbf{u}}}(i_t) di_t\,, \tag{A.3}$$

$$\sigma_{RR} = \text{Var}\{R\} = \int_{\mathcal{I}} i_r^2\, p_R(i_r) di_r - \text{E}^2\{R\}\,, \tag{A.4}$$

$$\sigma_{TT} = \text{Var}\{T_{\mathbf{u}}\} = \int_{\mathcal{I}} i_t^2\, p_{T_{\mathbf{u}}}(i_t) di_t - \text{E}^2\{T_{\mathbf{u}}\}\,, \tag{A.5}$$

$$\sigma_{RT} = \text{Cov}\{R, T_{\mathbf{u}}\} = \int_{\mathcal{I}^2} i_r\, i_t\, p_{R,T_{\mathbf{u}}}(i_r, i_t) di_r\, di_t - \text{E}\{R\}\,\text{E}\{T_{\mathbf{u}}\}\,, \tag{A.6}$$

where p_R and $p_{T_{\mathbf{u}}}$ denote the marginal intensity distributions estimated from R and $T_{\mathbf{u}}$, respectively, and $p_{R,T_{\mathbf{u}}}$ stands for an estimate of the joint intensity distribution. The intensities of the datasets, $i_r, i_t \in \mathcal{I} \subset \mathbb{R}$, are considered as random variables whose probability densities are respectively given by p_R and $p_{T_{\mathbf{u}}}$.

In order to obtain the external forces field related to the SSIM-based energy term (i.e., the first addend in the Euler-Lagrange equation (5)), the computation of the corresponding *Gâteaux*

derivative $d\mathcal{D}^{\text{SSIM}}$ is required. Therefore, we carry out an explicit computation from the definition of the *Gâteaux* derivative (see eq.(4)):

$$d\mathcal{D}^{\text{SSIM}}[R, T; \mathbf{u}; \mathbf{z}] = \frac{\partial}{\partial \epsilon} \left. \mathcal{D}^{\text{SSIM}}[R, T; \mathbf{u} + \epsilon \mathbf{z}] \right|_{\epsilon=0}$$

$$= -\frac{(\mu_R^2 + \mu_T^2 + C_1)(\sigma_{RR} + \sigma_{TT} + C_2)(2\mu_R \mu_T'(2\sigma_{RT} + C_2) + 2\sigma_{RT}'(2\mu_R \mu_T + C_1))}{(\mu_R^2 + \mu_T^2 + C_1)^2(\sigma_{RR} + \sigma_{TT} + C_2)^2}$$

$$+ \frac{(2\mu_R \mu_T + C_1)(2\sigma_{RT} + C_2)(2\mu_T \mu_T'(\sigma_{RR} + \sigma_{TT} + C_2) + \sigma_{TT}'(\mu_R^2 + \mu_T^2 + C_1))}{(\mu_R^2 + \mu_T^2 + C_1)^2(\sigma_{RR} + \sigma_{TT} + C_2)^2} \Bigg|_{\epsilon=0}$$

$$= \int_{\mathcal{I}^2} L_{\mathbf{u}+\epsilon\mathbf{z}}^{\text{SSIM}}(i_r, i_t) \frac{\partial}{\partial \epsilon} p_{R, T_{\mathbf{u}+\epsilon\mathbf{z}}}(i_r, i_t) di_r\, di_t \Bigg|_{\epsilon=0},$$

(A.7)

with $L_{\mathbf{u}+\epsilon\mathbf{z}}^{\text{SSIM}}$ being an intensity operator —whose definition, not necessary at this point, is not explicitly provided for the sake of simplicity—, and where the notation $(\cdot)' = \frac{\partial}{\partial \epsilon}(\cdot)$ is used.

Assuming a displacement $\mathbf{u} + \epsilon\mathbf{z}$, the joint intensity distribution estimated from R and $T_{\mathbf{u}+\epsilon\mathbf{z}}$ is provided by a non-parametric Parzen-Rozenblatt density model (Duda and Hart, 1973):

$$p_{R, T_{\mathbf{u}+\epsilon\mathbf{z}}}(i_r, i_t) = \frac{1}{\mathcal{V}_{\Psi}} \int_{\Psi} \hat{G}_\rho \left(R(\mathbf{x}) - i_r, T(\mathbf{x} + \mathbf{u}(\mathbf{x}) + \epsilon\mathbf{z}(\mathbf{x}) - i_t) \right) d\mathbf{x},$$

(A.8)

where $\mathcal{V}_{\Psi}$ denotes the hypervolume of Ψ and $\hat{G}_\rho : \mathcal{I}^2 \to \mathbb{R}$ is a Gaussian kernel (strictly positive and differentiable):

$$\hat{G}_\rho(i_r, i_t) = \frac{1}{2\pi\rho^2} e^{-\frac{i_r^2 + i_t^2}{2\rho^2}}.$$

(A.9)

At this point, derivatives of $p_{R, T_{\mathbf{u}+\epsilon\mathbf{z}}}$ can be easily computed. In particular,

$$\frac{\partial}{\partial \epsilon} p_{R, T_{\mathbf{u}+\epsilon\mathbf{z}}}(i_r, i_t) = \frac{1}{\mathcal{V}_{\Psi}} \int_{\Psi} \frac{\partial}{\partial i_t} \hat{G}_\rho \left(R(\mathbf{x}) - i_r, T(\mathbf{x} + \mathbf{u}(\mathbf{x}) + \epsilon\mathbf{z}(\mathbf{x})) - i_t \right) \nabla T(\mathbf{x} + \mathbf{u}(\mathbf{x}) + \epsilon\mathbf{z}(\mathbf{x})) \mathbf{z}(\mathbf{x}) d\mathbf{x}.$$

(A.10)

We now replace (A.10) in (A.7), and then let $\epsilon = 0$:

$$d\mathcal{D}^{\text{SSIM}}[R, T; \mathbf{u}; \mathbf{z}] = \frac{1}{\mathcal{V}_{\Psi}} \int_{\Psi} \int_{\mathcal{I}^2} L_{\mathbf{u}}^{\text{SSIM}}(i_r, i_t) \frac{\partial}{\partial i_t} \hat{G}_\rho \left(R(\mathbf{x}) - i_r, T(\mathbf{x} + \mathbf{u}(\mathbf{x})) - i_t \right) \nabla T(\mathbf{x} + \mathbf{u}(\mathbf{x})) \mathbf{z}(\mathbf{x}) di_r\, di_t\, d\mathbf{x}$$

$$= \int_{\Psi} \left\langle \frac{1}{\mathcal{V}_{\Psi}} \left(\hat{G}_\rho * \frac{\partial L_{\mathbf{u}}^{\text{SSIM}}}{\partial i_t} \left(R(\mathbf{x}), T(\mathbf{x} + \mathbf{u}(\mathbf{x})) \right) \right) \nabla T(\mathbf{x} + \mathbf{u}(\mathbf{x})), \mathbf{z}(\mathbf{x}) \right\rangle_{\mathbb{R}^d} d\mathbf{x}$$

$$= \int_{\Psi} \left\langle \mathbf{f}^{\text{SSIM}}(\mathbf{x}; \mathbf{u}), \mathbf{z}(\mathbf{x}) \right\rangle_{\mathbb{R}^d} d\mathbf{x}.$$

(A.11)

In the previous equation, a bidimensional convolution with respect to the intensity variable $\mathbf{i} = (i_r, i_t)$ appears naturally. This convolution conmutes with the derivative $\frac{\partial}{\partial i_t}$ (since both are linear operators). Moreover, by identifying the resulting expression with an inner product in $\mathbb{R}^d$, the external forces field of the Euler-Lagrange equation (5) which corresponds to the SSIM-based energy term can be finally obtained:

$$\mathbf{f}^{\text{SSIM}} = \frac{1}{\mathcal{V}_{\Psi}} \left(\hat{G}_\rho * \frac{\partial L_{\mathbf{u}}^{\text{SSIM}}}{\partial i_t} \right) \nabla T_{\mathbf{u}},$$

(A.12)

with

$$\frac{\partial L_{\mathbf{u}}^{\text{SSIM}}}{\partial i_t} = \frac{\gamma_0 + C_1\,\gamma_1 + C_2\,\gamma_2 + C_1 C_2\,\gamma_3}{(\mu_R^2 + \mu_T^2 + C_1)^2(\sigma_{RR} + \sigma_{TT} + C_2)^2}\,, \tag{A.13}$$

and where the definitions of γ_0, γ_1, γ_2 and γ_3 can be found in eqs.(7)-(10).

References

Amintoosi, M., Fathy, M., Mozayani, N., 2009. Precise image registration with structural similarity error measurement applied to superresolution. EURASIP Journal on Advances in Signal Processing 2009, 305479.

Amit, Y., 1994. A nonlinear variational problem for image matching. SIAM Journal of Scientific Computing 15, 207–224.

Bai, J., Feng, X.C., 2007. Fractional-order anisotropic diffusion for image denoising. IEEE Transactions on Image Processing 16, 2492–2502.

Ben Sassi, O., Delleji, T., Taleb-Ahmed, A., Feki, I., Ben Hamida, A., 2008. Mr image monomodal registration using structure similarity index, in: Image Processing Theory, Tools and Applications, 2008. IPTA 2008. First Workshops on, pp. 1–5.

Bookstein, F.L., 1989. Principal warps: thin-plate splines and the decomposition of deformations. IEEE Transactions on Pattern Analysis and Machine Intelligence 11, 567–585.

Brown, L.G., 1992. A survey of image registration techniques. ACM Computing Surveys 24, 325–376.

Brunet, D., Vrscay, E., Wang, Z., 2012. On the mathematical properties of the structural similarity index. Image Processing, IEEE Transactions on 21, 1488–1499.

Cachier, P., Bardinet, E., Dormont, D., Pennec, X., Ayache, N., 2003. Iconic feature based nonrigid registration: the PASHA algorithm. Computer Vision and Image Understanding 89, 272–298.

Charnoz, A., Agnus, V., Malandain, G., Forest, C., Tajine, M., Soler, L., 2005. Liver registration for the follow-up of hepatic tumors, in: Duncan, J., Gerig, G. (Eds.), Medical Image Computing and Computer-Assisted Intervention MICCAI. Springer Berlin / Heidelberg. volume 3750 of *Lecture Notes in Computer Science*, pp. 155–162.

Davis, P.J., 1979. Circulant Matrices. Wiley-Interscience, NY.

Duda, R., Hart, P., 1973. Pattern Classification and Scene Analysis. Wiley.

Elhawary, H., Oguro, S., Tuncali, K., Morrison, P., Shyn, P., Tatli, S., Silverman, S., Hata, N., 2009. Intra-operative multimodal non-rigid registration of the liver for navigated tumor ablation, in: Yang, G.Z., Hawkes, D., Rueckert, D., Noble, A., Taylor, C. (Eds.), Medical Image Computing and Computer-Assisted Intervention MICCAI. Springer Berlin / Heidelberg. volume 5761 of *Lecture Notes in Computer Science*, pp. 837–844.

Fischer, B., Modersitzki, J., 1999. Fast inversion of matrices arising in image processing. Numerical Algorithms 22, 1–11.

Fischer, B., Modersitzki, J., 2002. Fast diffusion registration. M.Z. Nashed, O. Scherzer (eds), Contemporary Mathematics 313, Inverse Problems, Image Analysis, and Medical Imaging, AMS , 117–129.

Fischer, B., Modersitzki, J., 2004. A unified approach to fast image registration and a new curvature based registration technique. Linear Algebra and its Applications 308, 107–124.

Frigo, M., Johnson, S.G., 2005. The design and implementation of FFTW3. Proceedings IEEE 93, 216–231.

Huang, Y.H., Ou, T.S., Su, P.Y., Chen, H., 2010. Perceptual rate-distortion optimization using structural similarity index as quality metric. Circuits and Systems for Video Technology, IEEE Transactions on 20, 1614–1624.

Johnson, H.J., Christensen, G.E., 2002. Consistent landmark and intensity-based image registration. IEEE Transactions on Medical Imaging 21, 450–461.

Kalinic, H., Loncaric, S., Bijnens, B., 2011. A novel image similarity measure for image registration, in: Image and Signal Processing and Analysis (ISPA), 2011 7th International Symposium on, pp. 195–199.

Klein, S., Staring, M., Murphy, K., Viergever, M.A., Pluim, J.P.W., 2010. elastix: A toolbox for intensity-based medical image registration. IEEE Transactions on Medical Imaging 29, 196–205.

Kolesov, I., Lee, J., Sharp, G., Vela, P., Tannenbaum, A., 2016. A stochastic approach to diffeomorphic point set registration with landmark constraints. IEEE Transactions on Pattern Analysis and Machine Intelligence 38, 238–251.

Lange, T., Wenckebach, T.H., Lamecker, H., Seebass, M., Hnerbein, M., Eulenstein, S., Gebauer, B., Schlag, P.M., 2005. Registration of different phases of contrast-enhanced ct/mri data for computer-assisted liver surgery planning: Evaluation of state-of-the-art methods. The International Journal of Medical Robotics and Computer Assisted Surgery 1, 6–20.

Larrey-Ruiz, J., Morales-Sánchez, J., 2006. Optimal parameters selection for non-parametric image registration methods. Lecture Notes in Computer Science 4179, 564–575.

Larrey-Ruiz, J., Morales-Sánchez, J., Verdú-Monedero, R., 2007. Generalized regularization term for non-parametric multimodal image registration. Signal Processing 87, 2837–2842.

Larrey-Ruiz, J., Verdú-Monedero, R., Morales-Sánchez, J., 2008. A fourier domain framework for variational image registration. Journal of Mathematical Imaging and Vision 32, 57–72.

Legaz-Aparicio, A.G., Verdú-Monedero, R., Larrey-Ruiz, J., Morales-Sánchez, J., López-Mir, F., Naranjo, V., Bernabéu, A., 2017. Efficient variational approach to multimodal registration of anatomical and functional intra-patient tumorous brain data. International Journal of Neural Systems (27), 1–10.

Loizou, C.P., Theofanous, C., Pantziaris, M., Kasparis, T., 2014. Despeckle filtering software toolbox for ultrasound imaging of the common carotid artery. Computer Methods and Programs in Biomedicine 114, 109 – 124.

Maintz, J., Viergever, M., 1998. A survey of medical image registration. Medical Image Analysis 2, 1–36.

Modersitzki, J., 2004. Numerical Methods for Image Registration. Oxford University Press, NY.

Murphy, K., van Ginneken, B., Reinhardt, J., Kabus, S., Ding, K., Deng, X., Cao, K., Du, K., Christensen, G., Garcia, V., Vercauteren, T., Ayache, N., Commowick, O., Malandain, G., Glocker, B., Paragios, N., Navab, N., Gorbunova, V., Sporring, J., de Bruijne, M., Han, X., Heinrich, M., Schnabel, J., Jenkinson, M., Lorenz, C., Modat, M., Mc-Clelland, J., Ourselin, S., Muenzing, S., Viergever, M., De Nigris, D., Collins, D., Arbel, T., Peroni, M., Li, R., Sharp, G., Schmidt-Richberg, A., Ehrhardt, J., Werner, R., Smeets, D., Loeckx, D., Song, G., Tustison, N., Avants, B., Gee, J., Staring, M., Klein, S., Stoel, B., Urschler, M., Werlberger, M., Vandemeulebroucke, J., Rit, S., Sarrut, D., Pluim, J., 2011. Evaluation of registration methods on thoracic ct: The empire10 challenge. Medical Imaging, IEEE Transactions on 30, 1901–1920.

Myronenko, A., Song, X., 2010. Intensity-based image registration by minimizing residual complexity. Medical Imaging, IEEE Transactions on 29, 1882–1891.

Naranjo, V., Morales, S., Legaz-Aparicio, A.G., Larrey-Ruiz, J., Bernabéu, A., Fuentes-Hurtado, F., 2015. A software for surgical and radiotherapy planning through multimodal brain image registration and fusion. International Journal of Computer Assisted Radiology and Surgery 10, 15–17.

Ou, Y., Akbari, H., Bilello, M., Da, X., Davatzikos, C., 2014. Comparative evaluation of registration algorithms in different brain databases with varying difficulty: Results and insights. Medical Imaging, IEEE Transactions on 33, 2039–2065.

Rehman, A., Wang, Z., Brunet, D., Vrscay, E., 2011. Ssim-inspired image denoising using sparse representations, in: Acoustics, Speech and Signal Processing (ICASSP), 2011 IEEE International Conference on, pp. 1121–1124.

Rohr, K., 2001. Landmark-based image analysis: using geometric and intensity models. Computational Imaging and Vision Series, Kluwer Academic Publishers, Dordrecht 21.

Sotiras, A., Davatzikos, C., Paragios, N., 2013. Deformable medical image registration: A survey. Medical Imaging, IEEE Transactions on 32, 1153–1190.

Sotiras, A., Ou, Y., Paragios, N., Davatzikos, C., 2015. Graph-based deformable image registration, in: Paragios, N., Duncan, J., Ayache, N. (Eds.), Handbook of Biomedical Imaging; Methodologies and Clinical Research. Springer. Lecture Notes in Computer Science (Book 779).

Tosun, D., Rettmann, M.E., Prince, J.L., 2004. Mapping techniques for aligning sulci across multiple brains. Medical Image Analysis 8, 295–309.

Urschler, M., Zach, C., Ditt, H., Bischof, H., 2006. Automatic point landmark matching for regularizing nonlinear intensity registration: application to thoracic CT images. Lecture Notes in Computer Science 4191, 710–717.

Verdú-Monedero, R., Larrey-Ruiz, J., Morales-Sánchez, J., 2008. Frequency implementation of the Euler-Lagrange equations for variational image registration. IEEE Signal Processing Letters 15, 321–324.

Vishnukumar, S., Wilscy, M., 2009. A comparative study on adaptive local image registration methods, in: 2009 International Conference on Signal Processing Systems, pp. 140–145.

Wang, J., Zhang, J.Q., 2009. An iterative refinement dsa image registration algorithm using structural image quality measure, in: Intelligent Information Hiding and Multimedia Signal Processing, 2009. IIH-MSP '09. Fifth International Conference on, pp. 973–976.

Wang, Z., Bovik, A.C., Sheikh, H.R., Simoncelli, E.P., 2004. Image quality assessment: from error visibility to structural similarity. IEEE Transactions on Image Processing 13, 600–612.

Wen, C., Wang, D., Shi, L., Chu, W.C.W., Cheng, J.C.Y., Lui, L.M., 2015. Landmark constrained registration of high-genus surfaces applied to vestibular system morphometry. Computerized Medical Imaging and Graphics 44, 1–12.

Wirth, M., Bobier, B., 2009. Registration of the prokudin-gorskii colour photographs using a multiresolution ssim algorithm, in: Kamel, M., Campilho, A. (Eds.), Image Analysis and Recognition. Springer Berlin Heidelberg. volume 5627 of *Lecture Notes in Computer Science*, pp. 917–926.

Zhang, Z., Jiang, Y., Tsui, H., 2006. Consistent multi-modal non-rigid registration based on a variational approach. Pattern Recognition Letters 27, 715–725.

Zitová, B., Flusser, J., 2003. Image registration methods: a survey. Image and Vision Computing 21, 997–1000.

15